J|A|C|S
ARTICLES
Published on Web 02/05/2008

Metal−Peptide Frameworks (MPFs): "Bioinspired" Metal Organic Frameworks

Alexandre Mantion,*,† Lars Massüger,‡ Pierre Rabu,§ Cornelia Palivan,† Lynne B. McCusker,‡ and Andreas Taubert*,†,||

Department of Chemistry, Klingelbergstrasse 80, University of Basel, CH-4056 Basel, Switzerland, Laboratory of Crystallography, ETH Zurich, CH-8093 Zurich, Switzerland, IPCMS UMR 7504 CNRS - Université Louis Pasteur, 23, rue du Loess, BP 43, F-67034 Strasbourg CEDEX 2, France, and Institute of Chemistry, University of Potsdam and Max-Planck-Institute of Colloids and Interfaces, D-14476 Golm, Germany

Received August 20, 2007; E-mail: ataubert@uni-potsdam.de; a.mantion@unibas.ch

Abstract: Chiral metal-organic frameworks (MOFs) have attracted a growing interest for their potential use in energy technologies, asymmetric catalysis, chiral separation, and on a more basic level, the creation of new topologies in inorganic materials. The current paper is the first report on a peptide-based MOF, a metal peptide framework (MPF), constructed from an oligovaline peptide family developed earlier by our group (Mantion, A.; et al. *Macromol. Biosci.* **2007**, *7*, 208). We have used a simple oligopeptide, Z-(L-Val)$_2$-L-Glu(OH)-OH, to grow porous copper and calcium MPFs. The MPFs form thanks to the self-assembling properties of the peptide and specific metal−peptide and metal−ammonia interactions. They are stable up to ca. 250 °C and have some internal porosity, which makes them a promising prototype for the further development of MPFs.

Introduction

Metal organic frameworks (MOFs) have attracted tremendous attention over the past few years. This is due to the fact that they are porous, have large surface areas of over 5000 m^2/g, and have tunable pores sizes and topologies.[1−4] MOFs are constructed from relatively simple organic building blocks, which act as connectors between transition metals or lanthanides. Because of their "infinite" connectivity, MOFs can be viewed as porous inorganic polymers.[5] Furthermore, like zeolites and aluminophosphates, MOFs are crystalline materials. However, whereas zeolites and other microporous materials are purely inorganic, MOFs are organic/inorganic hybrids. Despite the presence of organic building blocks, MOFs are robust materials. Their low density and high surface area are useful for gas sorption and energy technologies,[6,7] filtration,[8] or possibly even lightweight building materials. Other MOFs have useful optical[9] and electronic properties[10] or have been proposed as transport vessels for biological applications.[11]

MOFs can be synthesized using a wide variety of methods from hydrothermal to simple diffusion methods.[1,4,12,13] To date, most ligands used as connectors are rigid and do not carry additional functionalities, which could modify the properties of the MOF pores. There are only a few studies on flexible connectors and connectors that also self-assemble in the absence of a metal ion. For example, several groups have studied MOFs obtained from adipic acid, auxiliary bases, and Ca^{2+}, lanthanides, or 3d transition metals.[14−21]

Interestingly, there have been no reports on the use of peptides or peptidomimetics as connectors. This is particularly intriguing because peptide chemistry offers a virtually unlimited structural diversity, including additional metal coordinating sites, etc. Moreover, peptides are intrinsically chiral, which should make

† University of Basel.
‡ ETH Zurich.
§ IPCMS.
|| University of Potsdam.

(1) Yaghi, O. M.; Li, H.; Davis, C.; Richardson, D.; Groy, T. *Acc. Chem. Res.* **1998**, *31*, 474.
(2) Barton, T. J.; Bull, L. M.; Klemperer, W. G.; Loy, D. A.; McEnaney, B.; Misono, M.; Monson, P. A.; Pez, G.; Scherer, G. W.; Vartuli, J. C.; Yaghi, O. M. *Chem. Mater.* **1999**, *11*, 2633.
(3) James, S. L. *Chem. Soc. Rev.* **2003**, *32*, 276.
(4) Rowsell, J. L. C.; Yaghi, O. M. *Microporous Mesoporous Mater.* **2004**, *73*, 3.
(5) Robin, A. Y.; Fromm, K. M. *Coord. Chem. Rev.* **2006**, *250*, 2127.
(6) Rosi, N. L.; Eckert, J.; Eddaoudi, M.; Vodak, D. T.; Kim, J.; O'Keeffe, M.; Yaghi, O. M. *Science* **2003**, *300*, 1127.
(7) Duren, T.; Sarkisov, L.; Yaghi, O. M.; Snurr, R. Q. *Langmuir* **2004**, *20*, 2683.
(8) Chen, B.; Liang, C.; Yang, J.; Contreras, D. S.; Clancy, Y. L.; Lobkovsky, E. B.; Yaghi, O. M.; Dai, S. *Angew. Chem., Int. Ed.* **2006**, *45*, 1390.
(9) Fan, J.; Zhu, H.-F.; Okamura, T.-A.; Sun, W.-Y.; Tang, W.-X.; Ueyeama, N. *N. J. Chem.* **2003**, *27*, 1409.
(10) Ye, Q.; Song, Y.-M.; Wang, G.-X.; Chen, K.; Fu, D.-W.; Chan, W.; Hong, P.; Zhu, J.-S.; Huang, S. D.; Xiong, R.-G. *J. Am. Chem. Soc.* **2006**, *128*, 6554.
(11) Horcajada, P.; Serre, C.; Vallet-Regi, M.; Sebban, M.; Taulelle, F.; Ferey, G. *Angew. Chem., Int. Ed.* **2006**, *45*, 5974.
(12) Kitagawa, S.; Noro, S. *Compreh. Coord. Chem.* **2004**, *7*, 231.
(13) Clegg, W. *Compreh. Coord. Chem.* **2004**, *1*, 579.
(14) Borkowski, L. A.; Cahill, C. L. *Inorg. Chem.* **2003**, *42*, 7041.
(15) Borkowski, L. A.; Cahill, C. L. *Inorg. Chem. Commun.* **2004**, *7*, 725.
(16) de Lill, D. T.; Bozzuto, D. J.; Cahill, C. L. *Dalton Trans.* **2005**, 2111.
(17) de Lill, D. T.; Gunning, N. S.; Cahill, C. L. *Inorg. Chem.* **2005**, *44*, 258.
(18) Dimos, A.; Tsaousis, D.; Michaelides, A.; Skoulika, S.; Golhen, S.; Ouahab, L.; Didierjean, C.; Aubry, A. *Chem. Mater.* **2002**, *14*, 2616.
(19) Kiritsis, V.; Michaelides, A.; Skoulika, S.; Golhen, S.; Ouahab, L. *Inorg. Chem.* **1998**, *37*, 3407.
(20) Lobo, R. F.; Zones, S. I.; Davis, M. E. *J. Inclusion Phenom.* **1995**, *21*, 47.
(21) Kim, Y.; Suh, M.; Jung, D.-Y. *Inorg. Chem.* **2004**, *43*, 245.

Scheme 1. Oligovaline Peptides[a]

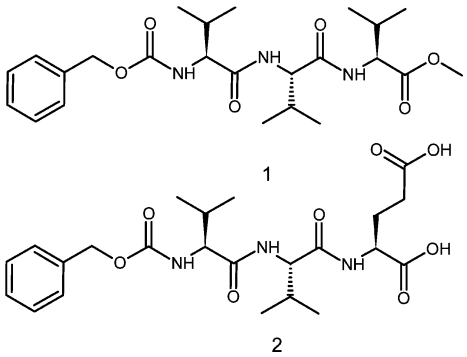

[a] **1** is the parent compound used in our earlier studies.[29,30] **2** is the peptide ligand used for construction of the MPFs and for magnetic dilution in the EPR experiments in the current paper.

them prime candidates for the fabrication of chiral MOFs. Chiral MOFs are, beyond the more fundamental search for new topologies, highly attractive as asymmetric catalysts, for chiral recognition, and applications requiring noncentrosymmetric crystal structures like nonlinear optical devices.[22−26]

There are essentially three approaches for the preparation of chiral MOFs: (i) the exploitation of molecules, where the chiral resolution happens without further assistance,[27] (ii) the use of chiral co-ligands in addition to achiral connectors,[23] or (iii) the use of a chiral connector.[25,28] The chiral connector approach is currently most often used because of its flexibility.[22−28]

We have recently introduced a family of self-assembling peptides based on oligovalines. These peptides gel a variety of solvents, including the inorganic liquid tetraethylorthosilicate (TEOS). Furthermore, they act as templates for complex titania and silver/peptide nanostructures.[29,30] The current paper shows that replacing one valine unit with a glutamic acid, Scheme 1, leads to peptides that can form peptide analogs of MOFs, which we have termed metal peptide frameworks (MPFs). The peptides form strong bonds with Cu^{2+} and Ca^{2+}, and the resulting crystalline materials precipitate from solution as long needle-like micrometer-sized particles.

Experimental

Materials. Amino acids were purchased from Bachem AG (Bubendorf, Switzerland), and all other chemicals were purchased from Fluka (Buchs, Switzerland). All chemicals were used as received.

Ligand Synthesis. The synthesis of the precursor peptide ZVVOH and of peptide **1** has been described elsewhere.[29]

Z-L-Val-L-Val-L-Glu(OtBu)OtBu. Isobutyl chloroformate (1.4 mL, 10.3 mmol) was added to a salt/ice cooled solution of Z-L-Val-L-Val-OH (3.0 g, 8.6 mmol) and 4-methylmorpholine (1.7 mL, 14.6 mmol) in 25 mL of acetonitrile under argon. The reaction mixture was stirred for 2 min. Then, 3.0 g (10.3 mmol) of L-glutamic acid di-tert-butyl ester hydrochloride and 1.7 mL (14.6 mmol) of 4-methylaminomorpholine were added. After 15 min, the cooling was removed and the solution was allowed to warm up to room temperature, upon which the solution was stirred for 24 h. The solvents were removed by rotary evaporation, and the residue was dissolved in 200 mL of chloroform. The organic solution was washed three times with 100 mL of a mixture of saturated hydrogen carbonate solution and sodium chloride, once with aqueous sodium chloride, three times with 100 mL of 10% citric acid and aqueous sodium chloride, and twice with aqueous sodium chloride. The organic phase was dried with sodium sulfate, concentrated to dryness, and the residue was triturated with pentane to give a white solid (3.4 g, 75%) after drying. IR (neat, cm^{-1}) 3479, 3277, 3063, 2976, 1633, 1533, 1429, 1393, 1371, 1349, 1283, 1247, 1222, 1153, 1088, 1071, 1038, 1028, 1020, 1005, 987, 920, 908, 864, 846, 799, 774, 753, 740, 698, 667. Elemental analysis calculated: C 62.92, H 8.35, N 7.10, O 21.63; measured: C 62.97, H 8.32, N 7.19. FAB-MS calculated $[M-H]^+ = 592$, measured $[M-H]^+ = 592$. ^{13}C NMR (δ in ppm vs TMS, d_6-DMSO, 100 MHz) 172.25, 171.84, 171.70, 171.51, 156.91, 137.96, 129.16, 128.56, 128.52, 128.45, 81.40, 80.56, 66.19, 61.11, 57.94, 52.58, 31.71, 31.12, 28.56, 28.43, 27.04, 20.11, 20.01, 18.99, 18.96. ^1H NMR (δ in ppm vs TMS, d_6-DMSO, 400 MHz) 8.23 (d, 0.9 H, H amide), 8.1 (d, 0.1 H, H amide), 7.92 (d, 0.1 H, H amide), 7.72 (d, 0.8 H, H amide), 7.33 (m, 6 H, H phenyl + H carbamate), 5.01 (s, 2 H, benzyl), 4.22 (t, 1 H, α Val-1), 4.12 (m, 1 H, α Val-2), 3.94 (m, 1 H, α Glu), 2.22 (m, 2 H, γ Glu), 1.92 (m, 3 H, β Val-1 + β Val 2 + β Glu), 1.72 (m, 1 H, β Glu), 1.36 (m, 18 H, tert-butyl ester x 2), 0.83 (m, 12 H, γ Val-1 + γ Val-2)

Z-L-Val-L-Val-L-Glu(OH)OH 2. Two grams of Z-L-Val-L-Val-L-Glu(OtBu)OtBu were reacted with 25 mL of a 95% aqueous trifluoroacetic acid (TFA) solution for 30 min under argon. Then the solvent was removed under reduced pressure. The residue was treated three times with 30 mL of chloroform. After evaporation of the chloroform, the slightly yellow solid was triturated with diethyl ether, filtered, and the whitish solid was dried overnight under vacuum, leaving 1.29 g of white solid **2** (80%). IR (neat, cm^{-1}) 3289, 3074, 2976, 1637, 1530, 1419, 1340, 1293, 1242, 1217, 1179, 1150, 1075, 1043, 1029, 995, 965, 934, 917, 859, 842, 798, 778, 756, 736, 697. FAB-MS: calculated $[M-H]^+ = 480$; measured $[M-H]^+ = 480$. Elemental analysis calculated: C 57.61, H 6.94, N 8.76, O 26.69; measured: C 56.91, H 6.90, N 8.60. ^1H NMR (δ in ppm vs TMS, d_6-DMSO, 400 MHz) 12.35 (very broad, 2 H, acidic protons), 8.17 (d, 0.94 H, H amide), 8.03 (d, 0.17 H, H amide), 7.90 (d, 0.12 H, H amide), 7.72 (d, 0.9 H, H amide), 7.36 (m, 6 H, H carbamate + H phenyl), 5.01 (s, 2 H, H benzylic), 4.18 (m, 2 H, α Val-1 + α Val-2), 3.92 (m, 1 H, α Glu), 1.94 (m, 3 H, 1H β-Glu + β Val-1 + β Val-2), 1.76 (m, 1 H, 1 H β Glu), 0.82 (m, 14 H, 2 H γ Glu + 6 H γ Val-1 + 6 H γ Val-2). ^{13}C NMR (δ in ppm vs TMS, d_6-DMSO, 100 MHz) 174.59, 173.91, 172.95, 171.82, 156.94, 137.95, 129.99, 129.39, 129.25, 66.20, 61.13, 58.13, 51.98, 31.63, 31.08, 30.80, 27.04, 20.08, 19.96, 19.03, 18.95.

Complex Synthesis. The metal complexes were prepared by dissolving peptide **2** in a 60/40 (v/v) ethanol/water mixture. The pH of the solution was adjusted to pH 8 with diluted aqueous ammonia. In a typical experiment, 56 μL of a 3 mM aqueous copper(II) or calcium nitrate solution were added to the ligand solution at room temperature under stirring. After copper or calcium salt addition, the pH was readjusted to 8. The copper complex (MPF-9) immediately precipitated, and the calcium complex (MPF-2) precipitated after 1 h at 80 °C. To complete the reaction, the reaction mixture was further reacted for 48 h at 80 °C in a closed vessel. Then, the solids were centrifuged, washed with ethanol, and dried under vacuum overnight. Various metal/peptide ratios were used during the synthesis, but all precipitates had a 1:1 metal/peptide stoichiometry. Yields were above 99%. Elemental analysis (MPF-2, $C_{23}H_{39}CaN_3O_{12}$) calculated: C 46.85, H 6.67, N 7.13, O 32.56, Ca 6.80; measured: C 47.80, H 6.29, N 7.57. Elemental analysis (MPF-9 corresponding to the dibasic form of **2** plus 1 Cu^{2+} plus 2

(22) Kesanli, B.; Lin, W.-B. *Coord. Chem. Rev.* **2003**, *246*, 305.
(23) Bradshaw, D.; Claridge, J. B.; Cussen, E. J.; Prior, T. J.; Rosseinsky, M. J. *Acc. Chem. Res.* **2005**, *38*, 273.
(24) Zang, S.; Su, Y.; Li, Y.; Zhu, H.; Meng, Q. *Inorg. Chem.* **2006**, *45*, 2972.
(25) Lin, W. *J. Solid State Chem.* **2005**, *178*, 2488.
(26) Sun, D.; Ke, Y.; Collins, D. J.; Lorigan, G. A.; Zhou, H.-C. *Inorg. Chem.* **2007**, *46*, 2725.
(27) Gao, E.-Q.; Yue, Y.-F.; Bai, S.-Q.; He, Z.; Yan, C.-H. *J. Am. Chem. Soc.* **2004**, *126*, 1419.
(28) Wu, C.-D.; Hu, A.; Zhang, L.; Lin, W. *J. Am. Chem. Soc.* **2005**, *127*, 8940.
(29) Mantion, A.; Taubert, A. *Macromol. Biosci.* **2007**, *7*, 208.
(30) Mantion, A.; Guex, G.; Foelske, A.; Mirolo, L.; Fromm, K. M.; Painsi, M.; Taubert, A. *Soft Matter*, **2008**, DOI: 10.1039=b712826f.

Table 1. X-Ray Powder Diffraction Data Collection

synchrotron facility	SNBL (Station B) at ESRF
wavelength	0.50007 Å
diffraction geometry	Debye−Scherrer
analyzer crystal	Si 111
sample	rotating 1.0 mm capillary
2θ range	1.020−30.501°
step size	0.003° 2θ
time per step	1.0 s

NH_3 plus 2 H_2O: $C_{23}H_{41}CuN_5O_{10}$), calculated: C 45.20, H 6.76, N 11.46, Cu 10.40, O 26.18; measured: C 45.98, H 6.38, N 10.39.

Spectroscopy. ^1H and ^{13}C NMR spectra were recorded on an Avance 400 MHz NMR spectrometer. Infrared spectra were obtained from the neat samples on a Shimadzu FTIR 8300 with a Golden Gate ATR unit. Spectra were recorded from 300 to 4500 cm^{-1} with a resolution of 1 cm^{-1}. FAB-MS spectra were taken on a Finnigan MAT 312.

Microscopy. Scanning electron microscopy was done on a Philips XL30 FEG ESEM operated at 10 kV. Samples were sputtered with gold or platinum prior to imaging.

X-Ray Diffraction. Powder diffraction patterns were measured on the Swiss-Norwegian Beamlines (SNBL) at the European Synchrotron Radiation Facility (ESRF) in Grenoble. Details of the data collection are given in Table 1.

Powder diffraction data analysis and interpretation. Powder diffraction patterns were indexed using Topas Academic.[31,32] Le Bail parameters extraction were performed using Fullprof.[33,34] Structures of the complexes were generated using FOX.[35,36] Crystal was used to correct some hydrogen positions.[37] The Final complex structure was refined using XRS-82.[38]

Voids Volume Evaluation. After refinement and before evaluating the voids size and position, nonrefined hydrogen atoms were added using the hydrogen addition functionality in Crystals[37] using an average C−H distance of 1 Å. Plotting and structure analysis was performed using Platon[39] and CrystalMaker (CrystalMaker Software Ltd).

Thermal Analysis. Thermogravimetric analysis (TGA) was done with a Mettler Toledo TGA/SDTA 851e from 25 to 550 °C with a heating rate of 10 °C/min in N_2.

SQUID Measurements. The magnetic properties of MPF-9 were investigated on neat powder samples with a Quantum Design MPMS-XL SQUID magnetometer between 1.8 and 300 K. The magnetic field strength was varied from −5 to +5 T. All magnetic data were corrected for diamagnetism of the sample and the sample holder. To evaluate the antiferromagnetic coupling between the neighboring Cu(II) centers, we analyzed the susceptibility by using a model of Heisenberg $S = {}^1/_2$ spin chains. Writing the exchange Hamiltonian $\hat{H} = -J\sum_{i,j}\hat{S}_i\hat{S}_j$, we used the expression of the susceptibility χT given in the literature.[41]

$$\chi T = \frac{N\mu_B{}^2 g^2(0.25 + 0.0750y + 0.15047y^2)}{k(1 + 0.9931y + 0.34427y^2 + 3.0313y^3)} \qquad (1)$$

In expression 1, $y = |J|/kT$, where J is the exchange interaction between electron spin moments S_i.

Electron Paramagnetic Resonance Spectroscopy. EPR spectroscopy was done on an EPR Bruker ElexSys E500 operating at 9.6 GHz spectrometer equipped with an Oxford Instruments cryostat. All complexes were measured as powders at 75 and 293 K. The complexes were magnetically diluted with **2** to a maximum extent of 10% of Cu(II). Spectra were recorded using 100 kHz modulation frequency and a microwave power of 0.5 to 2 mW. The diphenylpicrylhydrazyl (DPPH) radical was used as a field marker ($g = 2.0036$). The spectra for the Cu(II) species were simulated using Symfonia software (Bruker), which is based on a third-order perturbation theory treatment and assumes Gaussian shapes for the line width tensors. The isotopes were considered in their natural abundance for each spectrum.

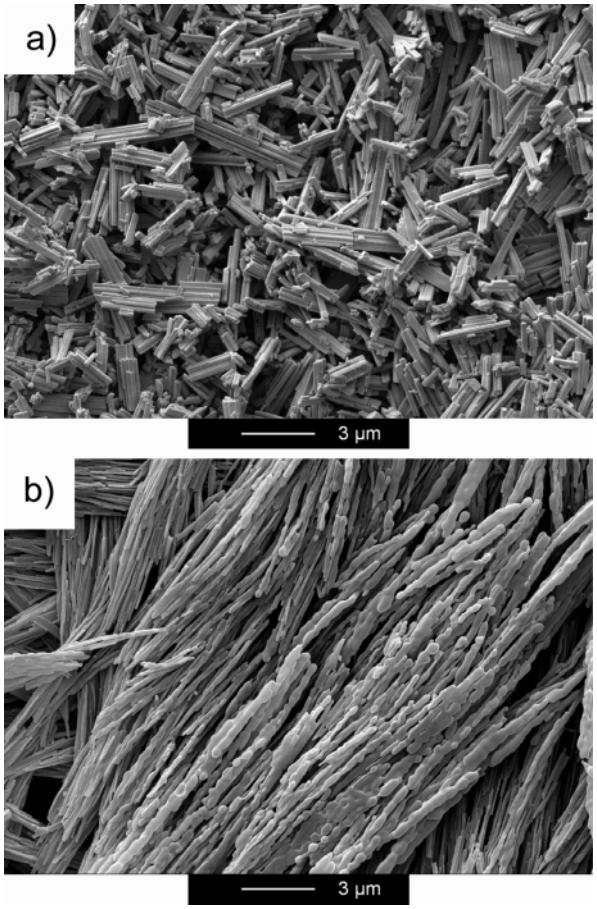

Figure 1. SEM images of (a) MPF-2 and (b) MPF-9.

Results and Discussion

Figure 1 shows representative scanning electron microscopy (SEM) images of the calcium complex MPF-2 and the copper complex MPF-9. Both samples have a fiber-like morphology with lengths ranging up to several micrometers and widths of ca. 200 nm. The calcium based MPF-2 crystals are somewhat shorter but have a more regular morphology with well developed crystal faces and edges. The copper-based MPF-9 appears less crystalline and seems to consist of smaller "blobs" that make up the rodlike particle.

Figure 2 shows thermogravimetric analysis (TGA) data. The pure ligand **2** exhibits a single sharp weight loss at 272 °C. There is no indication of the presence of water or other volatile substances, and no indication of decarboxylation. TGA curves of MPF-2 show four steps. The first one, at 35 °C, is relatively small (5%) and is caused by solvent or water evaporation. A clear weight loss of 19% is then observed at 262 °C. This weight loss is attributed to the loss of four molecules of water strongly bound in the crystal lattice or to solvent trapped in the structure. The third step is less clear and has an inflection point at

(31) Cheary, W.; Coelho, A. *J. Appl. Cryst.* **1992**, *25*, 109.
(32) Coelho, A. TOPAS; Academic 4.0 ed., 2006.
(33) Rodriguez-Carvajal, J. *Phys. B* **1993**, *192*, 55.
(34) http://www-llb.cea.fr/fullweb/fp2k/fp2k.htm, August 2006.
(35) Favre-Nicolin, V. R.; Cerny, R. *J. Appl. Cryst.* **2002**, *35*, 734.
(36) *Fox, Free Objects for Crystallography*, http://objcryst.sourceforge.net.
(37) Betteridge, P. W.; Carruthers, J. R.; Cooper, R. I.; Prout, K.; Watkin, D. J. *J. Appl. Cryst.* **2003**, *36*, 1487.
(38) Baerlocher, C. *The X-ray Rietveld System (XRS-82)*; ETH Zürich: Zürich, 1982.
(39) Spek, A. L. *J.Appl.Cryst.* **2003**, *36*, 7.
(40) Kueppers, H.; Liebau, F.; Spek, A. L. *J. Appl. Cryst.* **2006**, *39*, 338.
(41) Hatfield, W. E. *J. Appl. Phys.* **1981**, *52*, 1985.

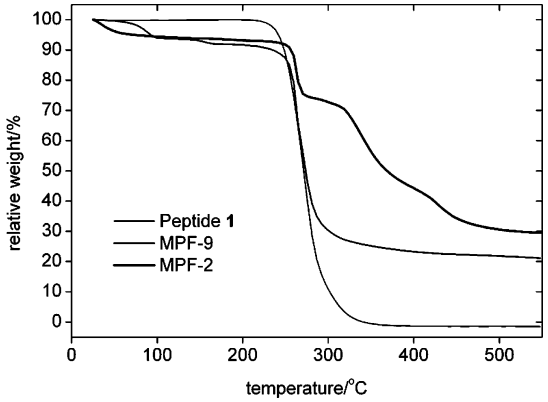

Figure 2. TGA curves of the pure peptide and the MPFs.

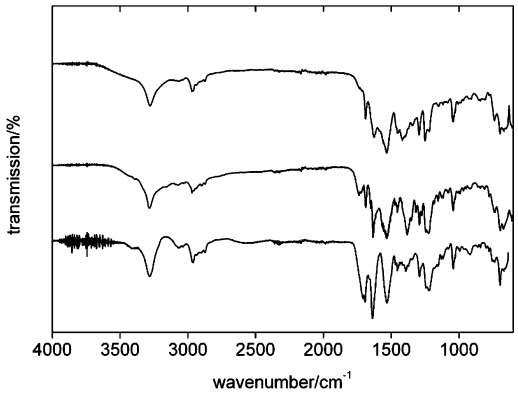

Figure 3. IR spectra of MPF-2 (top), MPF-9 (center), and pure peptide (bottom).

340 °C and a loss of 27%. The last weight loss of 14% is observed at 429 °C. The total mass loss indicates (assuming that Ca is present as CaO after TGA) that one Ca ion is bonded to one ligand molecule.

MPF-9 behaves similarly, except that there are only three thermal events. The first weight loss takes place at 91 °C, which is due to solvent evaporation. This weight loss of 6% is assigned to one equivalent of ethanol or two equivalents of adsorbed water. The second event occurs at 160 °C and is assigned to the loss of crystallographically bound solvent, most likely solvent molecules coordinated to the metal center. A final weight loss of 66% is observed at 260 °C. These data are consistent with a ratio of one copper to one ligand molecule, where the copper is possibly surrounded by one or two water or ammonia molecules (see elemental analysis and EPR results below, which suggest that two molecules of ammonia are bonded to the copper center) in the coordination sphere.

Figure 3 shows representative IR spectra of the pure peptide **2**, MPF-2, and MPF-9. The ligand bands at 3066, 1705, 1390, 1290, and 918 cm^{-1} can be assigned to O−H stretch, C═O stretch, C−O stretch, and O−H bending vibrations, respectively. Bands at 3280, 1637, 1528, and 1221 cm^{-1} can be assigned to the amide A, amide I, amide II, and amide III vibrations, respectively. The band at 1690 cm^{-1} can be attributed to the C═O vibration of the carbamate moiety. As in our previous work,[29] the amide band positions are indicative of a β-sheet structure. However, also as in our earlier work, IR does not reveal whether the organization of the β-sheet is parallel or antiparallel, because the diagnostic bands are obscured by vibrations of the *N*-benzylcarboxy group.[42,43] IR indicates that

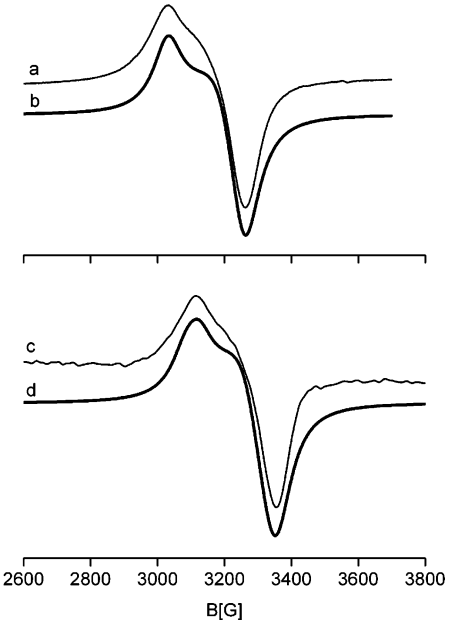

Figure 4. EPR spectra and spectrum simulations of MPF-9 powder measured at 75 and 293 K. (a) Spectrum measured at 75 K, (b) spectrum simulation, (c) spectrum measured at 293 K, and (d) spectrum simulation.

the β-sheet is conserved after reaction with calcium and copper, respectively, because the three bands at 1688, 1628, and 1533 cm^{-1} (MPF-2) and 1688, 1633, and 1533 cm^{-1} (MPF-9), indicative of the β-sheet, are still visible in the crystalline precipitates.

Besides the conservation of the β-sheet, IR also shows differences between the pure peptide and the metal complexes MPF-2 and MPF-9. After reaction of the ligand with the metal ions, the C═O stretch vibration of the glutamic acid at 1705 cm^{-1} disappears. This is in line with the fact that the ligand interacts with the metal ion via its acid moiety. Finally, differences between the peak positions of the asymmetric $\nu_{C=O}$ and the symmetric $\nu_{C=O}$ vibrations (1533 cm^{-1}, difference of 116 cm^{-1} in MPF-2, and 1564 cm^{-1}, difference of 182 cm^{-1} in MPF-9) suggest that a carboxylic acid acts as a bridging unit between metal centers in MPF-2 and as an asymmetric monodentate ligand in MPF-9.[44,45]

Figure 4 shows EPR spectra of MPF-9 powders measured at 75 and 293 K. Both spectra have an anisotropic overall shape, but because the signals are broad, the hyperfine pattern of Cu(II) is invisible. Therefore, simulation of the spectra was done using an orthorhombic gyromagnetic tensor, because a slight orthorhombic character of the gyromagnetic tensor has been previously obtained for other systems where Cu(II) was bonded to glutamic acid.[46] The hyperfine tensor could not be obtained due to the large linewidths. Table 2 summarizes the results from the simulation.

The presence of the half-field EPR signal shows that spin−spin interactions are present in MPF-9. This indicates, in accordance with the very low solubility of MPF-9 in organic

(42) Palumbo, M.; Da Rin, S.; Bonora, G. M.; Toniolo, C. *Makromol. Chem.* **1976**, *177*, 1477.
(43) Baron, M. H.; De Loze, C.; Toniolo, C.; Fasman, G. D. *Biopolymers* **1979**, *18*, 411.
(44) Deacon, G. B.; Phillips, R. J. *Coord. Chem. Rev.* **1980**, *33*, 227.
(45) Barth, A. P. *Prog. Biol. Mol. Biol.* **2000**, *74*, 141.
(46) Brondino, C. D.; Casado, N. M. C.; Passeggi, M. C. G.; Calvo, R. *Inorg. Chem.* **1993**, *32*, 2078.

Table 2. EPR Parameters Obtained by Simulating the Experimental Spectrum of MPF-9

		g					Γ/G		
complex	*T*/K	g_{xx}	g_{yy}	g_{zz}	g_{iso}	*A*	Γ_{xx}	Γ_{yy}	Γ_{zz}
MPF-9	75	2.082	2.113	2.235	2.143	–	55	80	62
	293	2.083	2.126	2.252	2.154	–	65	75	68

solvents, that there is a network of Cu(II) ions connected by bridging moieties. In most Cu complexes where the metal ions are bonded to two amino acid molecules this is realized by carboxylate as well as by hydrogen bond bridges. Both paths are in principle able to transfer spin polarization and therefore provide the dominant pathways for super-exchange.[46]

For two $S = {}^1/_2$ centers with gyromagnetic values near 2 and an electron−electron distance $r > 4.5$ Å, the integrated intensity of the half-field signal is determined only by the interspin distance *r*.[47] By assuming in this simple model that the anisotropic exchange is negligible, the integrated intensity ratio between the $\Delta MS = \pm 1$ and $\Delta MS = \pm 2$ transitions has been used to estimate a Cu(II)−Cu(II) distance of 5.75 Å. Because the gyromagnetic tensor is anisotropic, the anisotropic exchange interaction is not negligible, and therefore, the calculated electron−electron distance has an error of ca. 10%.

The values for the gyromagnetic tensor suggest that the first coordination sphere around the copper ion is distorted and involves, besides the oxygen atoms from the carboxylate groups, two nitrogen atoms. These two atoms are most likely from ammonia used in the synthesis of MPF-9. The distortion around the copper center is suspected to arise from the extended coordination ring of the glutamic acid moiety. This extended cycle is different from the more conventional 5-coordination ring in Cu(II)−L-arginine complexes where the 2N2O square planar geometry is preserved.[48] Moreover, these values indicate that the main contribution to the ground state wave function is given by the $d(x^2-y^2)$ orbital.

The EPR spectrum measured at 293 K exhibits the same shape, although the signal intensity slightly decreases. To simulate this spectrum, an octahedral gyromagnetic tensor and large linewidths, as in the case of low temperature measurements, were used. The values of the gyromagnetic tensor differ slightly from those obtained for the low temperature measurements but did not show a fluxional behavior of the copper ions.

The absence of any hyperfine structure has been previously observed for ferromagnetic chain complexes involving carboxylate bridges. There, carboxylate groups involving a copper-apical oxygen bond are more effective in transferring spin polarization than hydrogen bonds.[49] However, the relatively large electron−electron distance suggests that, in the case of MPF-9, the bridging does not involve carboxylate, but hydrogen bonds, which stabilize the hybrid system by forming long copper−copper 1-D chains. Moreover, the observed spectra are clearly different from spectra observed for copper(II) complexes of linear-chain fatty acids.[50]

Besides EPR, magnetic measurements were used to further characterize MPF-9. Figure 5 shows a Curie−Weiss plot of

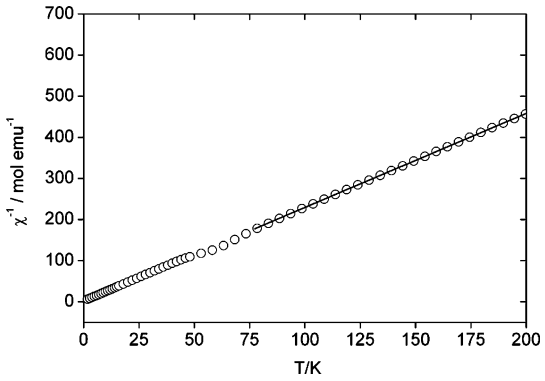

Figure 5. Curie−Weiss Plot of MPF-9.

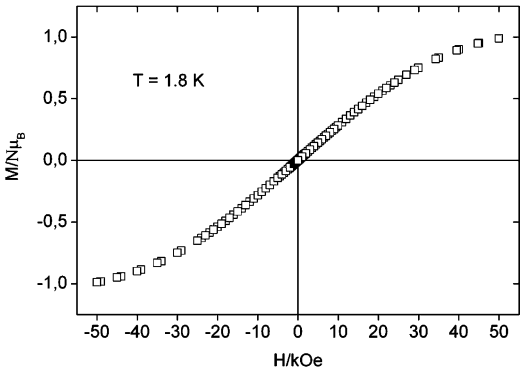

Figure 6. Magnetization versus field curve for MPF-9 recorded at 1.8 K.

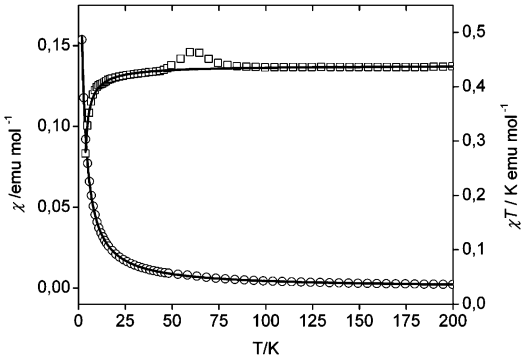

Figure 7. Temperature variation of the magnetic susceptibility, χ (○) and of the χ*T* product (□) of MPF-9 recorded in a 5000 Oe field. The full line corresponds to the fit carried out with the expression for Heisenberg $S = {}^1/_2$ chains.

MPF-9, and Figure 6 shows the corresponding saturation curve recorded at 1.8 K. The χ^{-1} dependence of *T* in the Curie−Weiss plot and the saturation curve clearly show that the structure is composed of $S = {}^1/_2$ Cu(II) ions and constitutes 1D Heisenberg $S = {}^1/_2$ chains.[51] The Curie−Weiss law is well-followed, and the fittings leads to $C = 0.437$ K cm^3 mol^{-1} and $\theta = -0.30$ K.

Figure 7 shows the corresponding χ*T* vs *T* curve. χ is almost constant down to 50 K and is well fitted using the Hattfield model of 1D Heisenberg $S = {}^1/_2$ chains.[41] A small hump at 50−60 K, not observed in the susceptibility vs *T* curve, was revealed when plotting the χ*T* product variation. This can be attributed either to very small amount of impurity or to the presence of oxygen, the signal of which is apparent due to the low mass of sample used for the measurement (3.2 mg). This anomaly however does not prevent interpreting the global

(47) Eaton, S. S.; More, K. M.; Sawant, B. M.; Eaton, G. R. *J. Am. Chem. Soc.* **1983**, *105*, 6560.
(48) Ohata, N.; Masuda, H.; Yamauchi, O. *Inorg. Chim. Acta* **1999**, *286*, 37.
(49) Colacio, E.; Ghazi, M.; Kivekas, R.; Moreno, J. M. *Inorg. Chem.* **2000**, *39*, 2882.
(50) Sharrock, P.; Dartiguenave, M.; Dartiguenave, Y. *Bioinorg. Chem.* **1978**, *9*, 3.
(51) Carlin, R. L. *Magnetochemistry*; Springer: Berlin-Heidelberg, 1986.

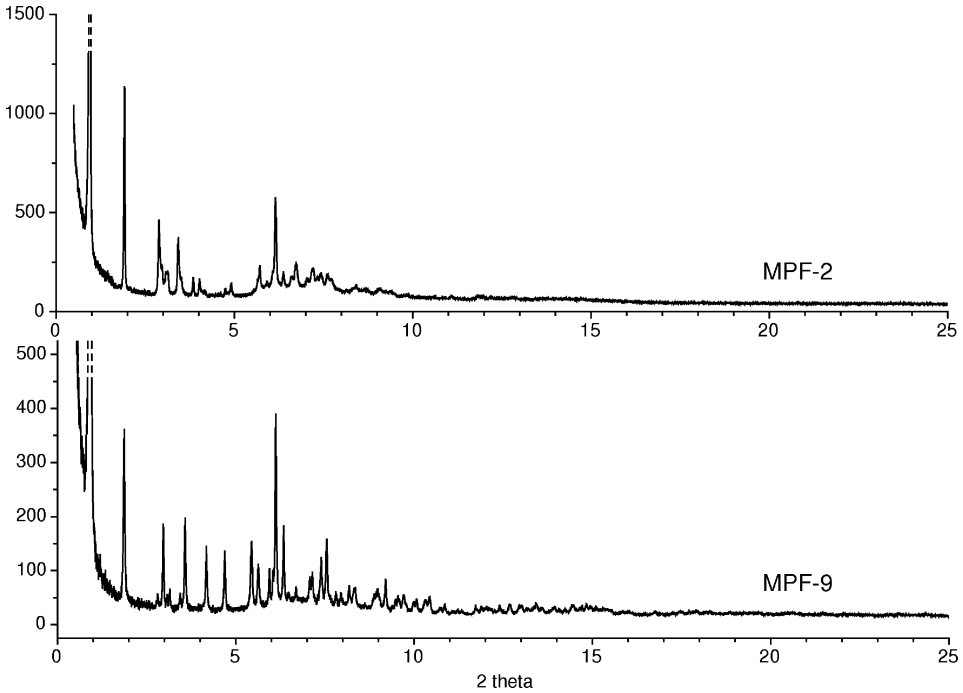

Figure 8. Synchrotron powder diffraction patterns of MPF-9 and MPF-2 ($\lambda = 0.50007$ Å). In both cases, the first peak has been cut at approximately 25% of its full height to show more detail at higher angles.

Table 3. Unit Cells for MPF-2 and MPF-9

sample	*a* (Å)	*b* (Å)	*c* (Å)	α (deg)	*β* (deg)	*γ* (deg)	space group
MPF-2	13.6714	9.7210	29.9315	90	94.826	90	monoclinic *P*
MPF-9	19.2610	4.8885	30.5096	90	92.524	90	monoclinic *C*2

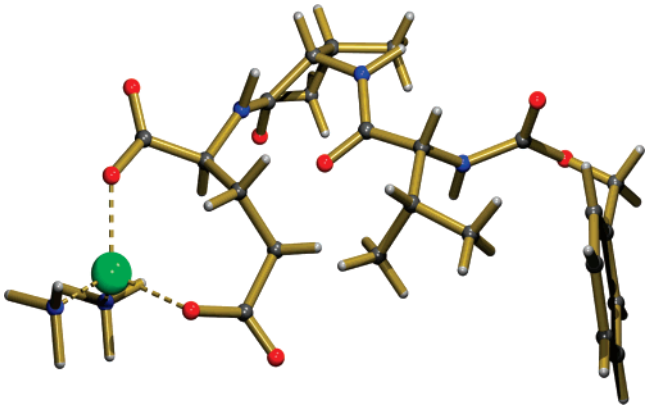

Figure 9. Crystal structure of MPF-9 generated by FOX and before Rietveld refinement, including hydrogen atoms.

Scheme 2. Chemical Structure Used as Input for FOX Analysis

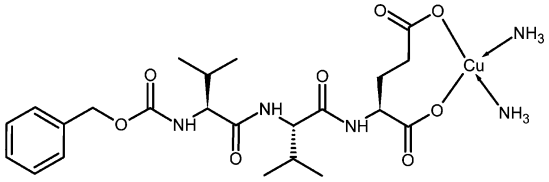

3

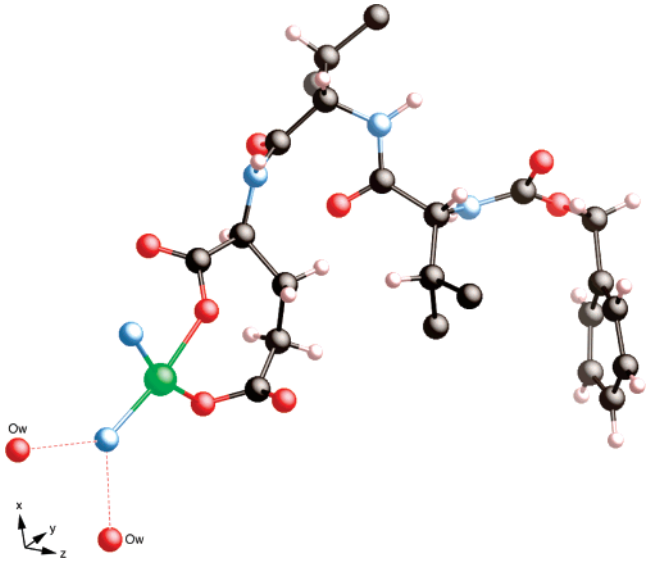

Figure 10. Crystal structure of MPF-9 after refinement of the model generated by FOX, including the water molecule.

behavior of MPF-9. Fitting of the curve leads to $g = 2.164(1)$ and $J/k = -1.38(1)$ K. The negative J value is characteristic for a weak antiferromagnetic coupling, as already observed from the EPR data.[52]

Both values are of the same order of magnitude and are in good agreement with the EPR values, as is the small Curie−Weiss constant θ. A small decrease in the χT product θ is observed from 0.437 K cm^3 mol^{-1} at 295 K to 0.283 K cm^3 mol^{-1} at 1.8 K. The decrease of χT and the negative sign of θ confirm the existence of small antiferromagnetic exchange

(52) Rodriguez-Fortea, A.; Alemany, P.; Alvarez, S.; Ruiz, E. *Chem.−Eur. J.* **2001**, *7*, 627.

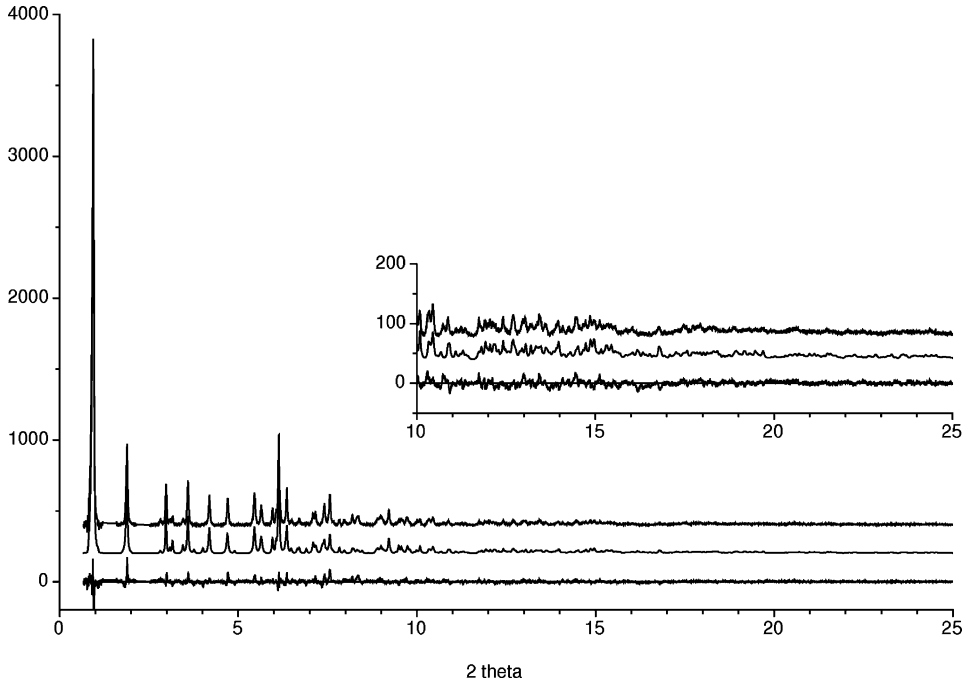

Figure 11. Observed (top), calculated (middle), and difference (bottom) profiles for the Rietveld refinement of MPF-9. The inset has been scaled up by a factor of 5 to show more detail.

interactions.[53] The weak *J* value confirms that the magnetization exchange occurs through nitrogen atoms and H-bonds and not through carboxylate-mediated interactions like in amino-acid copper(II) complexes.[54] As the behavior of complexes with a single carboxylate bridge indicates that *J* vanishes at distances over 3 Å because the direct interaction predominates over the superexchange mechanism, we exclude a single carboxylate bridge network in the case of MPF-9.[52]

Because neither MPF-2 nor MPF-9 crystallize as single crystals, powder diffraction methods had to be used for structure solution. The X-ray powder diffraction patterns for MPF-2 and MPF-9 are shown in Figure 8. They were indexed using Topas academic[31,32] and the results are shown in Table 3.

The quality of the powder diffraction pattern for MPF-2 did not allow structure solution. However, the powder pattern does suggest a lamellar structure. The peaks at 2θ values of 0.9068, 1.92, 2.88, and 3.88° (d-spacings of 29.85, 14.91, 9.95, and 7.46 Å) can be indexed as 001, 002, 003, and 004. This indicates a lamellar structure perpendicular to the *c* direction, which in turn suggests a β-sheet structure.

The diffraction pattern of MPF-9 was of better quality, and a crystal structure model could be obtained using the direct-space global-optimization algorithms implemented in the computer program FOX.[35,36] The chemical information used as input for these optimizations (connectivity, bond distances and angles) is shown in Scheme 2. Le Bail extraction was performed to determine Cagliotti parameters and the η ratio with Fullprof using a Pseudo-Voigt profile.[33,34] The best of the several copper complex structures generated by FOX is shown in Figure 9. Elemental and thermogravimetric analyses indicated that there is at least one water molecule per copper ion present in the structure, but to keep the model as simple as possible, this was not included in the FOX simulations. Some of the torsion angles were fixed or restricted to a certain range to limit the possibility of unrealistic torsion angles. For the optimization, data to sin $\theta/\lambda = 0.20$ (11.5° 2θ) were used. To allow for the steric requirements of the hydrogen atoms, they were included in the model submitted to Fox.

Table 4. Rietveld Refinement of MPF-9

unit cell	
space group	*C*2
a (Å)	19.2665(10)
b (Å)	4.8848(2)
c (Å)	30.5146(21)
β (deg)	92.5(1)
refinement	
number of observations	4723
number of contributing reflections	1107
number of geometric restraints	207
number of positional parameters	
non-H	113
H	57
number of profile parameters	11
R_F	0.103
R_{wp}	0.266
R_{exp}	0.217

To complete and refine the model from FOX, a Rietveld refinement using the program XRS-82[37] was undertaken. The complete diffraction pattern was used, and bond distance and angle restraints were included to keep the model chemically sensible. H atoms were added where their positions could be calculated from the connected atoms, but for the ammonia molecules and methyl groups, where the positions of the H atoms are not well defined, the occupancy factor for the corresponding N and C atoms were simply increased to include the three electrons from the attached H atoms (e.g., CH_3 was modeled as 1.5 C) and the atomic displacement factor increased slightly. During the course of the refinement, the weight of the geometric restraints with respect to the diffraction data was reduced progressively, and in the final stages a factor of 1.0

(53) Zou, J.-Z.; Liu, Q.; Xu, Z.; You, X.-Z.; Huang, X.-Y. *Polyhedron* **1998**, *17*, 1863.
(54) Gerard, M. F.; Aiassa, C.; Casado, N. M. C.; Santana, R. C.; Perec, M.; Rapp, R. E.; Calvo, R. *J. Phys. Chem. Solids* **2007**, *68*, 1533.

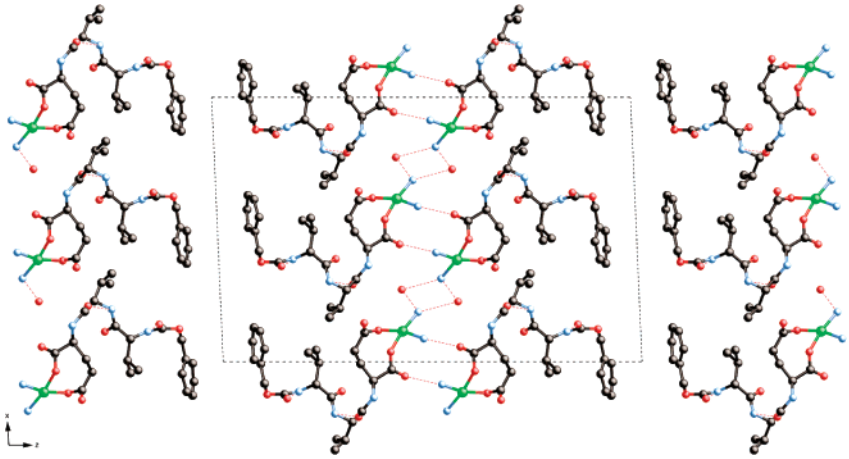

Figure 12. Packing scheme of the crystal. View slightly off the crystallographic *b*-axis. Hydrogen atoms have been removed for clarity.

was applied. A water molecule was located in a difference electron density map and added to the structural model as an O atom with an occupancy of 1.25 (to account for the two unlocated H atoms). To keep the number of parameters to a minimum, the atomic displacement parameters were fixed at typical values and not refined. Refinement of this model converged with the R-values $R_F = 0.103$, $R_p = 0.211$ and $R_{wp} = 0.266$ ($R_{exp} = 0.217$). The crystal structure including the water molecule is shown Figure 10. The profile fit is shown in Figure 11. Further details of the refinement are given in Table 4. The atom numbering convention is given in the Supporting Information, Figure S1. Atomic positions are given in Table S1, selected interatomic distances are given in Table S2, and bond angles are given in Table S3. Platon's CALC Void[40] function log journal is given in Table S4.

The copper ion is coordinated to two oxygens of the carboxylic acid and to two ammonia molecules introduced during the synthesis in a distorted square planar geometry. The Cu−N distances of 1.98(3) and 1.99(3) Å are in accordance with the generally observed values of 1.90−2.02 Å. Similarly, the Cu−O distances of 1.98(3) and 1.99(3) Å correspond to those observed in related systems.[55−58] A global view of the crystal structure of MPF-9 is shown in Figure 12, and a magnified view along the crystallographic *a*-axis in Figure 13. Both figures show that there are multiple interactions present in MPF-9. The water molecule forms H-bonds with ammonia molecules of neighboring Cu complexes along the [100] direction (N···O 2.88(5) and 3.02(4) Å) to create a helical H-bonding network along the [010] direction (Figure 14 and Supporting Information Figure S2). The other ammonia molecule forms H-bonds with the L-glutamic acid residue of the neighboring Cu complex along the [001] direction (N···O 2.87-(4) Å). There are two further H-bonds linking the peptides along the [010] direction (N···O 2.84(4) Å and N···O 3.01(4) Å). This dense hydrogen-bonding network accounts for the insolubility of this material in both water and organic solvents. The structure is, within the limitations of the method, very well-defined. It is also consistent with the results of the elemental analysis, TGA, EPR, and magnetic measurements.

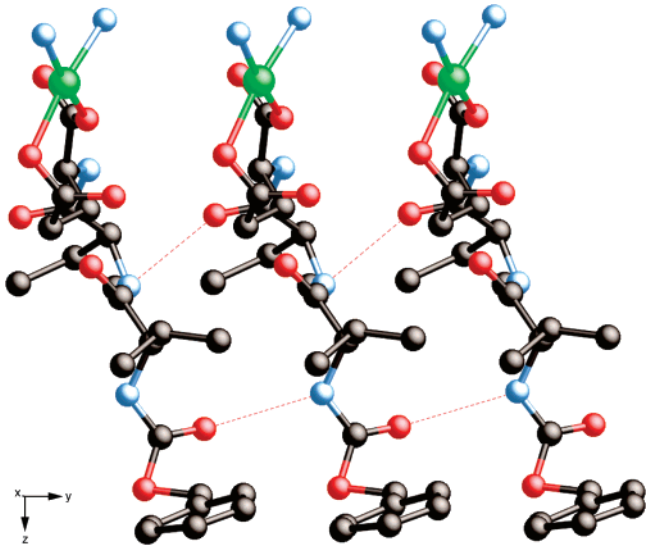

Figure 13. β-sheet-like structure and hydrogen bonding in the peptide backbone of MPF-9. Hydrogen atoms have been removed for clarity and N···O interactions are indicated by a dotted line.

The structure can be described in terms of two 2D substructures, which are interconnected via hydrogen bonding. However, there is no extended Cu(II) 3D network. The first substructure is composed of a double layer of copper ions in the *ab* plane that are diagonally displaced with respect to one another. Along [010], the copper(II) centers are separated by a distance of 4.9 Å and along [100], by 6.2 Å and 10.0 Å. Such a structure is in line with the magnetic properties of the material, which exhibits a weak antiferromagnetism and thus long Cu(II)−Cu(II) distances. Because of the spacing of the Cu(II) centers, the magnetic transfer cannot be based on carboxylate pathways, and must therefore be based on hydrogen bonding. Despite the existence of hydrogen bonds between adjacent complexes, there is no magnetic coupling between them, because the large number of atoms involved in the hydrogen-bonding network limits the magnetic interaction. The large distance of 6.2 Å between two columns of copper (II) as well as the packing of the ligands prevents any magnetic interactions between them and is in line with the modeling of the magnetic properties as a Heisenberg $S = {}^1/_2$ 1D chain.

(55) Devereux, M.; McCann, M.; Cronin, J. F.; Ferguson, G.; McKee, V. *Polyhedron* **1999**, *18*, 2141.
(56) Chawla, S. K.; Nättinen, K.; Rissanen, K.; Yakhmi, J. V. *Polyhedron* **2004**, *23*, 3007.
(57) Rodriguez-Martin, Y.; Ruiz-Pérez, C.; Sanchiz, J.; Lloret, F.; Julve, M. *Inorg. Chim. Acta* **2001**, *318*, 159.
(58) Li, J.; Zeng, H.; Chen, J.; Wang, Q.; Wu, X. *Chem. Commun.* **1997**, 1213.

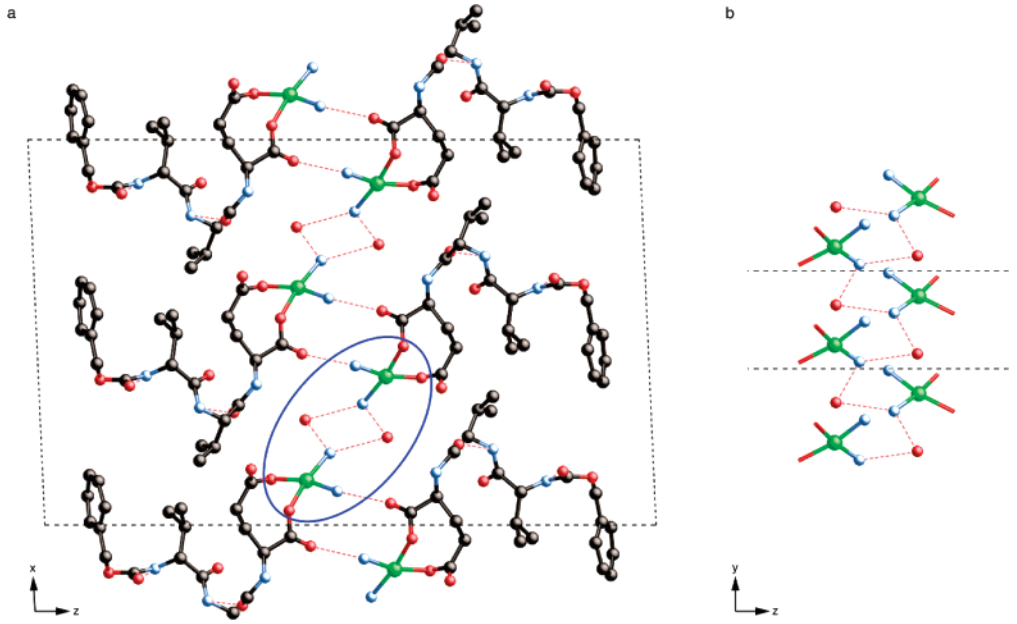

Figure 14. Hydrogen-bonding network in the *ac* plane (left) and a perpendicular view of the helical linkage between water and ammonia molecules along [010] (right). The hydrogen atoms have been removed for clarity.

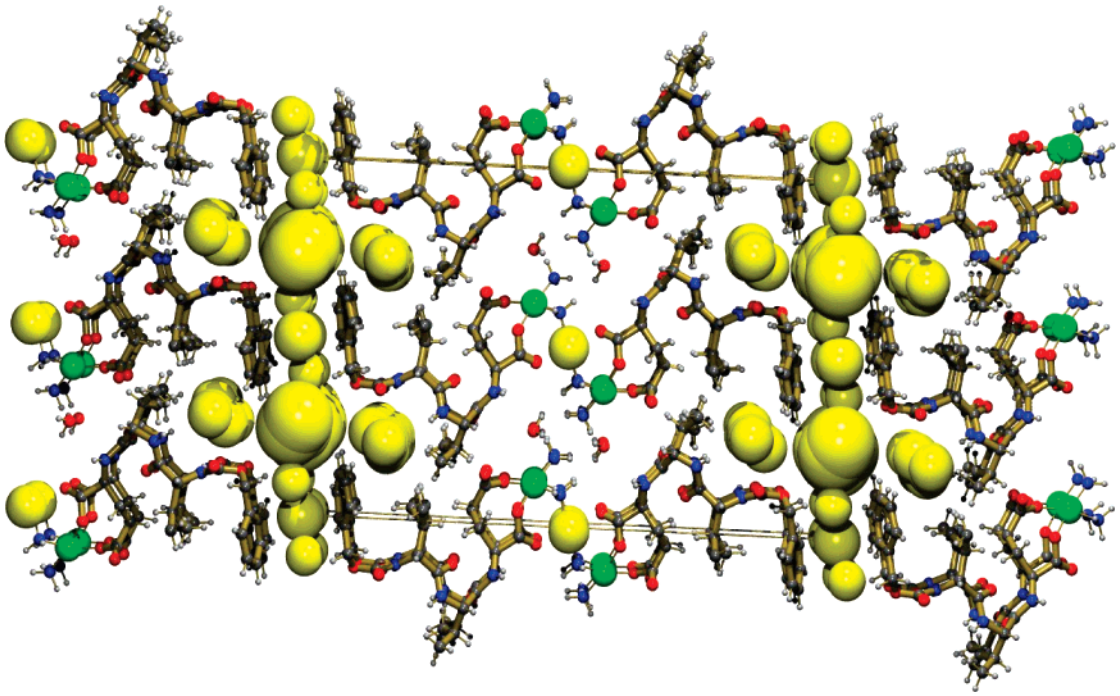

Figure 15. Packing diagram of MPF-9. Yellow balls indicate the voids.

The second double layer in the *ab* plane is that of the peptide with its long molecule axis oriented roughly along [001]. In addition to the H-bonding between the peptides along [010], the phenyl rings form a column along [010]. The centers of gravity of the individual phenyl residues are 4.9 Å apart, indicating some $\pi-\pi$-stacking interaction. The intercolumn distances are in the same range and the rings form a zigzag arrangement, which implies that $\pi-\pi$ stacking is responsible for both the internal and external column stabilization.

The hydrogen-bonding scheme adopted by the peptides in the crystal is shown in Figure 13. There is a β-sheet-like interaction along the crystallographic *b*-axis. The presence of a β-sheet bonding scheme has also been shown by IR spectroscopy (Figure 3), but the crystal structure further shows that not all of the peptide is part of the β-sheet. Only the carbamate and the L-valine-L-valine peptide bond are involved. To maximize the number of hydrogen bonds, the β-sheet is distorted slightly to accommodate the rather large side chains of the valine units. This distortion enables the L-glutamic acid residue to adapt to the metal center coordination geometry. The crystallographic results confirm those of the IR spectroscopy, and also reveal a more complex bonding scheme than simple β-sheets. Furthermore, the crystal structure shows that the β-sheet orientation, which could not be determined from IR, is parallel and not antiparallel along the *b*-axis.

The hydrogen bonding between the water and coordinated ammonia molecules that connects copper centers in adjacent columns is shown in Figure 14. This hydrogen-bonding scheme is an effective pathway for transferring magnetization through hydrogen bonding.[46,59] The structure presented here is a new mode of coordination for the well-known glutamic acid ligand,[46,49,60−62] where there is no magnetic exchange through carboxylate centers, although here the glutamic acids are not involved in a peptide-like structure. However, the gain in energy given by the formation of β-sheets via hydrophobic interaction, hydrogen bonding, and extensive $\pi-\pi$ stacking of benzyl rings is highly favorable and compensates the effect of the nonclassical bonding scheme.

The porosity of MPF-9 was analyzed using Platon's voids calculation functionality and plotting.[40] Figure 15 shows the pores in MPF-9 that are accessible to small solvent or gas molecules. The total void volume is 387 Å^3 for a total unit cell volume of 2867 Å^3. This results in a total void volume of just above 13% of the cell volume. MPF-9 only has chiral channel-like pores parallel to the [010] direction, but two ranges of sizes can be distinguished. The larger pores have a volume of around 101 Å^3. This is large enough to accommodate methanol, ethanol, or possibly benzene if the linear molecular shape of the latter three and the possible $\pi-\pi$ interactions are considered. The smaller voids are around 20−37 Å^3. These pores are large enough to accommodate hydrogen and carbon dioxide, or even water (in the pores at the larger end of the spectrum). However, the small connections between the 20 Å^3 voids prevent them from forming an extended channel along the *b*-axis. As a result, MPF-9 is a candidate for gas adsorption and storage, for purification, or for chiral separation.

In summary, metal−peptide frameworks are a new and interesting variety of metal-organic frameworks. The coordination mode of MPF-9 differs from other $\alpha-\omega$ dicarboxylic acids. There is no bridging of the carboxylic acid moiety between the metal centers as seen in refs 14−21. The current paper therefore suggests that peptides with different topologies should, like regular organic dicarboxylic acids, allow for the fabrication of MPFs with different topologies with specifically designed (chiral) inner pores. The ligand acts as a chelator, similar to smaller dicarboxylic acids like malonates.[55,56] This is rather surprising but can be rationalized via the overall energy gain from the formation of a highly hydrogen-bonded network with $\pi-\pi$-stacking. This energy gain is presumably higher than the energy gained by forming an extensive carboxylate network.

Furthermore, the synthesis conditions are convenient and there is no need for autoclave, microwave, or slow diffusion synthesis protocols, which are often used for MOF's.[5] The ease of synthesis is an important point for any industrial application. Although the overall cost of MPFs is somewhat higher than that of conventional MOFs, the ability to include chiral information and possibly other chemical information like metal coordinating sites *a priori* should alleviate issues of higher cost.

MPF-2 and MPF-9 are just the first examples of MPFs. They demonstrate that new peptide-based materials can be generated using rather simple building blocks and low strength, noncovalent interactions like hydrogen bonding[63,64] and $\pi-\pi$ stacking of benzyl rings,[65,66] along with metal complexation. A structurally interesting point is the role of the amines located around the copper(II). They not only complete the coordination sphere but also constitute a way of ensuring the stabilization and weak magnetization transfer in a metal column using hydrogen bonding. Moreover, $\pi-\pi$ stacking is very useful in stabilizing and organizing the complexes.

Conclusion

This paper presents the first example of metal−peptide frameworks, "bioinspired" analogs to the well-known MOFs. Metal−oxygen and metal−nitrogen bonding and various types of hydrogen bonding along with $\pi-\pi$-stacking are responsible for the formation of a porous network structure, which is stable up to ca. 250 °C. Despite the lack of single crystals, the crystal structure of the copper complex MPF-9 could be determined from powder diffraction data using the FOX program. The refined crystal structure is consistent with the spectroscopic information.

The 1D channel architecture with two different pore sizes makes MPF-9 an interesting material for gas storage. Further applications include gas or chiral separation or catalysis. Finally, the organization of the Cu(II) ions in a 2D layer pattern yields a material with an interesting paramagnetic character. The current paper therefore clearly shows that small peptides are viable candidates for the preparation of complex metal-organic materials with defined topologies. MPFs thus further broaden the more general field of MOFs and entactic metal systems,[67] which are interesting for a wide range of technical applications.

Acknowledgment. We thank Prof. E.C. Constable for access to his IR spectrometer, M. Düggelin and D. Mathys for SEM measurements, Prof. K. Fromm for access to her TGA, Prof. M. Meuwly for the access to one of his Linux clusters, F. Schmid for FOX and IT support, Dr. R. Černý and Dr. V. Favre-Nicolin for FOX support, J. Rohlíček providing a computer-grid capable FOX version, and Dr. Markus Neuburger for useful discussions. Experimental assistance from the staff at SNBL is gratefully acknowledged. The Swiss National Science Foundation, the NCCR Nanosciences, the University of Potsdam, and the Max-Planck-Institut of Colloids and Interfaces are acknowledged for financial support. A.T. thanks the Holcim Stiftung Wissen for a Habilitation Fellowship.

Supporting Information Available: Figures S1 and S2 and Tables S1−4. This material is available free of charge via the Internet at http://pubs.acs.org.

JA0762588

(59) Levstein, P. R.; Calvo, R. *Inorg. Chem.* **1990**, *29*, 1581.
(60) Steren, C. A.; Gennaro, A. M.; Levstein, A. M.; Calvo, P. R. *Condens. Matter* **1989**, *1*, 637.
(61) Colacio, E.; Dominguez-Vera, J. M.; Costes, J. P.; Kivekas, R.; Laurent, J. P.; Ruiz, J. *Inorg. Chem.* **1992**, *31*, 774.
(62) Pushita, W. J.; Odani, A.; Yamauchi, O. *J. Inorg. Biochem.* **1999**, *73*, 203.
(63) Beatty, A. M. *Cryst. Eng. Commun.* **2001**, 243.
(64) Katsura, N.-K. *Chem. Soc. Rev.* **2005**, *34*, 109.
(65) Roesky, H. W.; Andruh, M. *Coord. Chem. Rev.* **2003**, *236*, 91.
(66) Ye, B.-H.; Tong, M.-L.; Chen, X.-M. *Coord. Chem. Rev.* **2005**, *249*, 545.
(67) Comba, P. *Coord. Chem. Rev.* **2000**, *200−202*, 217.